International Journal of Mass Spectrometry 430 (2018) 37–43

Contents lists available at ScienceDirect

International Journal of Mass Spectrometry

journal homepage: www.elsevier.com/locate/ijms

Non-symbiotic hemoglobin conformational space dependence on the heme coordination using nESI-TIMS-TOF MS

David Butcher[a], Sophie Bernad[b], Valerie Derrien[b], Pierre Sebban[b], Jaroslava Miksovska[a,c], Francisco Fernandez-Lima[a,c,*]

[a] Department of Chemistry & Biochemistry, Florida International University, Miami, FL, USA
[b] Laboratoire de Chimie Physique, CNRS, Univ. Paris-Sud, Université Paris Saclay, 91405, Orsay, France
[c] Biomolecular Sciences Institute, Florida International University, Miami, FL, USA

ARTICLE INFO

Article history:
Received 18 August 2017
Received in revised form 9 January 2018
Accepted 21 March 2018
Available online 23 March 2018

Keywords:
Trapped ion mobility spectrometry
Rice type 1 non-symbiotic hemoglobin
Collision cross section
Unfolding

ABSTRACT

In this study, for the first time, the conformational space of the rice non-symbiotic hemoglobin type 1 (rHb1) was studied as a function of the starting solution pH using trapped ion mobility spectrometry coupled to mass spectrometry (TIMS-MS) and molecular dynamics. Comparison of the charge state distribution, apo to holo form ratio, and the collision cross section (Ω) profiles as a function of the solution pH showed higher stability of the rHb1 wild-type (WT) when compared with the H73L mutant at mildly acidic conditions. Comparison of the Ω profiles of the rHb1 WT and H73L holo and apo form showed that only the initial unfolding pathways involved the heme cavity, with and without a heme loss, followed by unfolding pathways not necessarily involving the environment of the heme prosthetic group. Candidate structures for the nine transitions observed in the Ω profiles were proposed using molecular dynamic simulations based on the Ω profiles, UV absorption spectroscopy and circular dichroism data as way to describe a potential unfolding pathway. The described unfolding pathway suggests that the rHb1 unfolding is driven by initial distancing of the A, B, and H helices, while the heme cavity and heme group remains intact, followed by the distancing of the E, F, and G helices and subsequent loss of the α-helical structure leading to a final random coil conformation.

© 2018 Elsevier B.V. All rights reserved.

1. Introduction

Non-symbiotic hemoglobins (nsHbs) are a class of heme proteins found in land plants which exhibit bis-histidyl coordination of the heme iron and can reversibly bind gaseous ligands, including carbon monoxide (CO), dioxygen (O_2), and nitric oxide (NO) [1]. NsHbs are localized in the cytoplasm of plant cells and share a 3-over-3 α-helical structure with a variety of other heme proteins. The heme B cofactor is found within a hydrophobic cavity in the protein referred to as the heme pocket [2]. NsHbs are closely related to symbiotic hemoglobins (sHbs), a class of heme proteins which participates in nitrogen fixation in the root nodules of leguminous plants through symbiotic interactions with *rhizobia* bacteria [3]. However, unlike sHbs, the functions of nsHbs *in vivo* are not fully understood. *In vitro*, nsHbs carry out an NO dioxygenase function, converting cytotoxic NO to nitrate (NO_3^-) by addition of O_2 [4]; this activity has led to the idea that detoxification of NO through NO dioxygenase activity is the primary function of nsHbs. NsHbs also typically exhibit a very high affinity for exogenous gaseous ligands; type 1 nsHb from rice (rHb1) has an affinity of ~1 nM for O_2 [1], showing stronger binding then that of the oxygen sensor protein FixL (~50 μM) suggesting that nsHbs may also act as oxygen sensors [5]. Expression of rHb1 is upregulated during seed germination and in differentiating plant tissues raising the possibility that nsHbs participate in developmental signaling by modulating levels of NO within the cell [6]. The rHb1 expression is also upregulated under conditions of etiolation (lack of sunlight) or hypoxia, suggesting that nsHbs are part of the cellular response to various stress conditions [7].

Previous studies using photoacoustic calorimetry (PAC) and transient absorption spectroscopy (TA) have shown the kinetics and energetics associated with CO photo dissociation from rHb1 WT and a distal histidine mutant, H73L, to be pH-dependent [8]. The use of mildly acidic conditions results in slower ligand migration from the protein matrix after photolysis of the iron-ligand bond. Classical molecular dynamics (cMD) simulations suggested that protonation of histidine residues within the protein leads to

* Corresponding author at: Department of Chemistry & Biochemistry, Florida International University, Miami, FL, USA.
E-mail address: fernandf@fiu.edu (F. Fernandez-Lima).

https://doi.org/10.1016/j.ijms.2018.03.008
1387-3806/© 2018 Elsevier B.V. All rights reserved.

reorganization of the CD-loop and EF-helical regions and restructuring of hydrophobic cavities within the protein, which are critical for migration of gaseous ligands between the solvent and the heme active site. Therefore, the structural changes induced by histidine protonation may be a mechanism by which enzymatic activity of the protein is affected by modulating interactions of the protein with gaseous ligands. Histidine protonation could occur as a result of pH changes in the cytoplasm of plant cells directly caused by the etiolation, hypoxia, and other stress conditions [9].

With the recent introduction of trapped ion mobility spectrometry coupled to mass spectrometry (TIMS-MS) [10,11], several studies have taken advantage of the high mobility resolving power (R ~400) for the separation of complex mixtures and structural characterization of biomolecules [12–24]. Several studies have shown the advantages of TIMS-TOF MS for the characterization of kinetically trapped intermediates as a function of the starting solution (e.g., pH and organic content) and collision induced activation prior to TIMS-TOF MS analysis [25–27]. In particular, we have previously shown that TIMS-TOF MS when complemented with molecular dynamics is a powerful tool for the study of heme proteins (e.g., myoglobin and cytochrome c) [28,29].

In the present work, we explore for the first time the potential of nESI-TIMS-TOF MS to study the kinetically-trapped intermediates of rHb1 wild type (WT) and H73L mutant as a function of the solution pH, ranging from 4.9 to 8.0. Complementary molecular dynamic simulations were utilized to generate potential protein structures with collision cross sections (Ω) similar to those observed experimentally.

2. Methods and materials

2.1. RHb1 expression and purification

The rHb1 WT and H73L mutant with poly-histidine tags were expressed recombinantly in *E. coli* strain BL21 and purified using Ni^{2+} affinity chromatography [1]. The rHb1 WT and H73L amino acid sequences and molecular weight are contained in Table S1. Proteins were dialyzed extensively against 20 mM HEPES buffer at pH 7.0 and stored in 200 μL aliquots at −80 °C. Prior to nESI-TIMS-MS analysis, proteins were extensively dialyzed into 10 mM ammonium acetate using 3 kDa (Amicon Ultra) and/or 10 kDa (Microcon-10) MWCO centrifugal filter units as needed. The solution pH was adjusted to 4.9 and 8.0 using 0.001% v/v acetic acid (Fisher Scientific) and 0.006% v/v triethylamine (Sigma), respectively. All samples were studied within 24 h of preparation to avoid protein degradation.

2.2. Trapped ion mobility spectrometry – mass spectrometry analysis

Individual rHb1 proteins were analyzed by directly infusing the sample via nESI into the TIMS-TOF MS spectrometer. A detailed overview of the TIMS analyzer and its operation can be found elsewhere [10,30,31]. The nitrogen bath gas flow is defined by the pressure difference between entrance funnel (P_1 = 2.6 mbar) and the exit funnel (P_2 = 1.0 mbar) at *ca.* 300 K. The TIMS analyzer is comprised of three regions: an entrance funnel, analyzer tunnel (46 mm axial length), and exit funnel. A 880 kHz and 200 Vpp RF potential was applied to each section creating a dipolar field in the funnel regions and a quadrupolar field inside the tunnel. In TIMS operation, multiple ion species are trapped simultaneously at different E values resulting from a voltage gradient applied across the TIMS tunnel, typically V_{ramp} = −280–0 V for low resolution scans and ΔV_{ramp} = 40–80 V for high resolution scans. Deflector ($V_{deflector}$), capillary ($V_{capillary}$), entrance funnel (V_{funnel} in) and end of the tunnel regiont (V_{out}) were set to 60, 50, 0 and 60 V respectively to avoid ion heating prior to TIMS analysis. The mobility, K, of an ion in a TIMS cell is described by:

$$K = v_g/\mathrm{E} = A/(V_{elution}\text{-}\mathrm{V_{out}}) \quad (1)$$

where v_g and E are the gas velocity and applied electric field. $V_{elution}$ and V_{out} are the elution voltage and voltage at the end of the tunnel region. A is an instrumental parameter determined by calibration using standards of known mobility. After thermalization, species are eluted from the TIMS cell by decreasing the electric field in stepwise decrements (referred to as the "ramp") and can be described by a characteristic elution voltage ($V_{elution}$). Eluted ions are then mass analyzed and detected by a maXis impact Q-ToF MS (Bruker Daltonics Inc, Billerica, MA).

In a TIMS device, the total analysis time can be described as:

$$\begin{aligned} TotalIMStime &= t_{trap} + (\mathrm{V_{elution}}/\mathrm{V_{ramp}}) * \mathrm{t_{ramp}} + TOF \\ &= t_o + (\mathrm{V_{elut}}/\mathrm{V_{ramp}}) * \mathrm{t_{ramp}} \end{aligned} \quad (2)$$

where, t_{trap} is the thermalization/trapping time, *TOF* is the time after the mobility separation, and V_{ramp} and t_{ramp} are the voltage range and time required to vary the electric field, respectively. The elution voltage was experimentally determined by varying the ramp time (t_{ramp} = 100–500 ms) for a constant ramp voltage setting. This procedure also determines the time ions spend outside the separation region, t_o (e.g., ion trapping and time-of-flight). The TIMS cell was operated using a fill/trap/ramp/wait sequence of 10/10/100-500/50 ms. The ToF analyzer was operated at 10 kHz (m/z 50–3500). The data was summed over 100 analysis cycles yielding an analysis time of ~50 s for the largest trapping times (t_{ramp} = 500 ms). Mobility calibration was performed using the Tuning Mix calibration standard (G24221A, Agilent Technologies, Santa Clara, CA) in positive ion mode (e.g., m/z 322, K_0 = 1.376 $cm^2\,V^{-1}\,s^{-1}$ and m/z 622, K_0 = 1.013 $cm^2\,V^{-1}\,s^{-1}$) [31]. The TIMS operation was controlled using in-house software, written in National Instruments Lab VIEW, and synchronized with the maXis Impact Q-ToF acquisition program. A custom-built source using pulled capillary nESI emitters was utilized for all the experiments. Quartz glass capillaries (O.D.: 1.0 mm and I.D.: 0.70 mm) were pulled utilizing a P-2000 micropipette laser puller (Sutter Instruments, Novato, CA) and loaded with 10 μL aliquot of the sample solution. A typical nESI source voltage of +700–1500 V was applied between the pulled capillary tips and the TIMS-TOF MS instrument inlet. Ions were introduced via a stainless-steel inlet capillary (1/16 × 0.020″, IDEX Health Science, Oak Harbor, WA) held at room temperature into the TIMS cell.

Reduced mobility values (K_0) were correlated with collision cross section (Ω) using the equation:

$$\Omega = \frac{(18\pi)^{1/2}}{16}\frac{z}{(k_B T)^{1/2}}\left[\frac{1}{m_i}+\frac{1}{m_b}\right]^{1/2}\frac{1}{K_0}\frac{1}{N^*} \quad (3)$$

where z is the charge of the ion, k_B is the Boltzmann constant, N^* is the number density of the bath gas and m_i and m_b refer to the masses of the ion and bath gas, respectively [32]. TIMS-MS spectra were analyzed using Compass Data Analysis 5.0 (Bruker Daltonik GmbH) and TIMS Data Viewer 1.4.0.31397 (Bruker Daltonik GmbH).

2.3. UV and CD measurements

The UV spectra of rHb1 WT and H73L were measured using a Biotek Synergy H1 hybrid multi-mode plate reader (Winooski, VT) using a Take3 micro volume plate from 2 μL volume of ~15 μM protein solution. The circular dichroism (CD) spectra of rHb1 WT and H73L were measured using a Jasco J-815 CD spectrophotometer (Oklahoma City, OK). The solution pH (5.0–8.0) was adjusted

using 0.1% v/v acetic acid (Fisher Scientific) and 0.006% v/v triethylamine (Sigma). The solution pH was measured at each point using a Thermo Scientific Orion Star A111 pH meter (Beverly, MA).

2.4. Molecular dynamics and theoretical collision cross section calculation

Candidate structures were generated using AMBER03 force field [33] in YASARA software following a candidate structure generation algorithm [34]. This approach is similar to that previously described by Fernandez-Lima et al. for peptides [35], with the main characteristic that the initial search targets the generation of the identity vectors, followed by charge assignment and energy minimization. The X-ray crystal structure PDB 1D8U was modified to include the extended N-terminal containing the poly-histidine tag utilized in the experiments (see full rHb1 WT and H73L sequences in Table S1) and used as initial guess for the native rHb1 form in the molecular dynamics. A loop modeling feature was utilized to enhance the unfolding of the α-helices and nine structures were selected from the conformational ensemble as representatives of the main conformational transitions weighted by the root-mean-square deviation (RMSD) relative to the previous unfolding step; the later step simplifies the curation of the unfolding steps that can describe the Ω band transitions of interest. Notice that these candidate structures are used as a simplified way to evaluate the unfolding pathway; that is, other structures/pathways are also possible and could agree with the experimental mobility trends. Theoretical ion-neutral Ω values were calculated using Collidoscope software version 1.3 and utilized the charge placement algorithm [36].

3. Results and discussion

The nESI-TIMS-TOF MS analysis of rHb1 WT and H73L as a function of the starting solvent conditions (pH = 4.9–8.0) showed a wide charge state distribution (+8–+21 charge states) and a wide

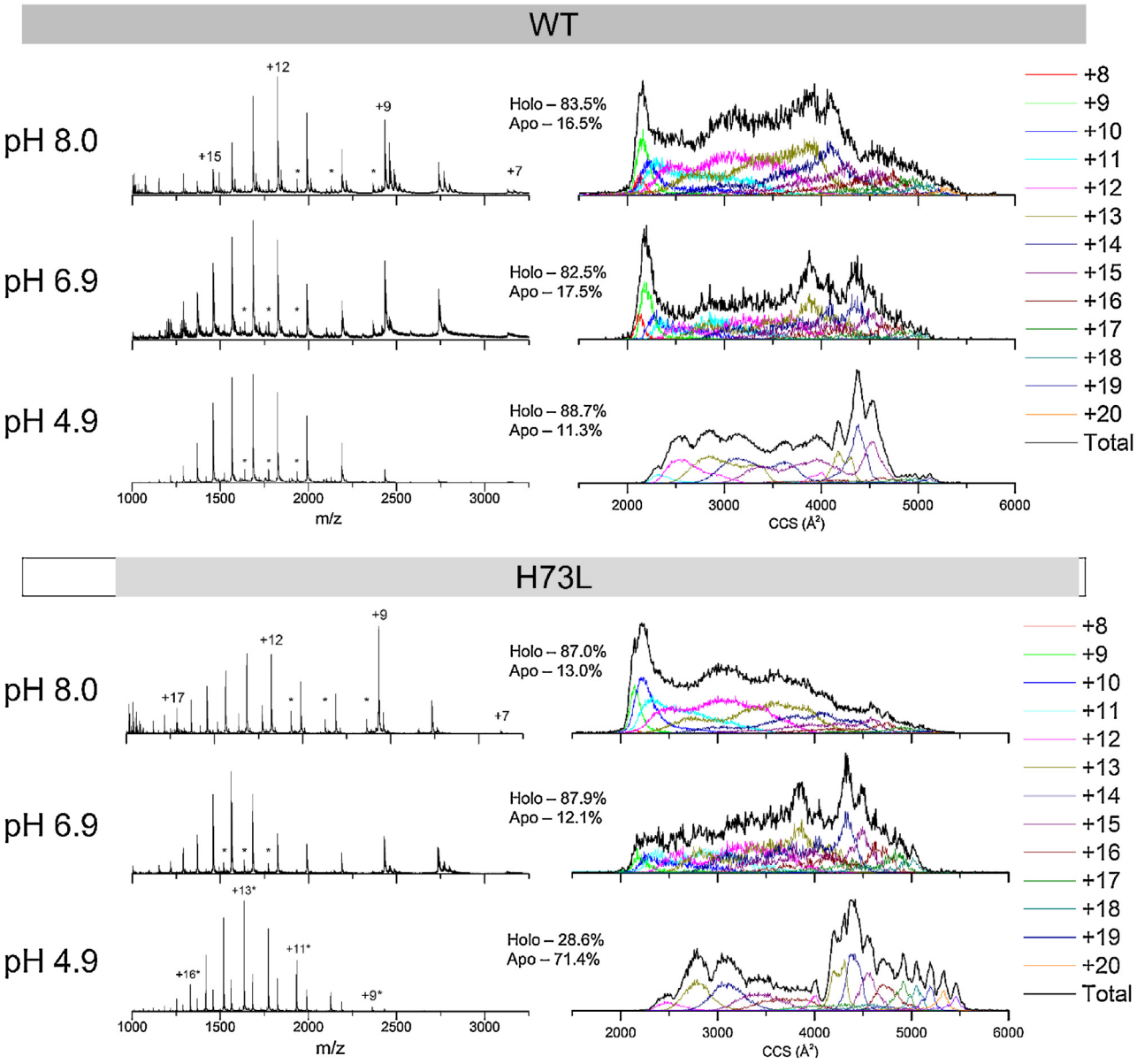

Fig. 1. Typical positive mode mass spectra (left) and CCS profiles (right) for rHb1 WT (top) and rHb1 H73L (bottom) at pH 8.0, 6.9, and 4.9. Mass spectra peaks corresponding to the apoprotein are marked with asterisks. Notice the higher structural stability of the rHb1 WT at lower pH indicated by the holo to apo ratio.

Ω range (2000–5500 Å^2), similar to previous studies of equine myoglobin and cytochrome c using TIMS and other mobility platforms [19,28,29,37–42]. Inspection of the charge state distribution as a function of the starting solution conditions showed the highest abundance of the lower charge states and lower Ω values under basic conditions (pH = 8.0) with a shift towards higher charge states and higher Ω with decreasing pH. It has been previously observed that proteins undergoing electrospray ionization from neutral solution tend to populate a limited number of low charge states [43]. This reflects the predominance of the natively-folded protein in the solution phase, as the native protein has fewer ionizable residues which are exposed to the solvent. Conversely, higher charge states are observed for various partially-unfolded protein species due to increased solvent accessibility of ionizable amino acid residues. The observation of higher charge states (≥+11) for rHb1 WT and H73L therefore reflects the presence of unfolded conformations in solution at all solution pH values. The increased prevalence of higher charge states and larger Ω values for both proteins under neutral and acidic conditions indicates that the protein structure is destabilized by decreasing pH. This is in good agreement with previous pH- and/or organic content-driven unfolding pathways for biomolecules studied using TIMS-MS [25,28,29].

Also during the electrospray process, evaporation of water molecules from nanodroplets can result in a significant decrease in pH. In the case of ammonium acetate buffer being sprayed in positive mode, the pH is estimated to decrease to ~4.75, close to the pK_a of acetate [44]. The significant differences between the mobility profiles resolved at an initial solution pH of 6.9 and 4.9 suggest that under our experimental conditions the pH of the protein microenvironment does not change significantly between spraying and desolvation of the protein, or that the brief exposure of the protein to more acidic conditions within the drying nanodroplet is not sufficient to impact the mobility distributions.

Comparison of the Ω profile dependence of rHb1 WT and H73L on the starting solvent conditions suggests that the transition from native to molten globule as the solution pH decreases occurs first for the rHb1 H73L mutant compared to the WT (Fig. 1). Moreover, the rHb1 WT and H73L mutant proteins were observed in both the apo and holo forms across the entire range of charge states, with a higher abundance of the holo form for rHb1 WT regardless of the pH condition; a more significant transition from holo to apo form was observed for the rHb1 H73L mutant as the pH decreases. It should be noted that a higher heme ligand affinity is observed for rHb1 WT and H73L mutant when compared with similar experiments performed with myoglobin at mildly acidic conditions [28] where the holoprotein was only observed at the lowest charge states (+8 and +9).

The higher stability of the rHb1 WT when compared to the H73L mutant at mildly acidic conditions suggests that the higher the coordination number the more the heme ligand is retained in the cavity (e.g., hexa vs penta coordinated) and the higher the protein resistance to unfolding. Complementary CD analysis of rHb1 WT and H73L as a function of the solution pH showed very similar overall trends between the two proteins (Fig. 2). Inspection of the molar ellipticity (θ) and its first derivative (dθ/dpH) showed that rHb1 WT and H73L mutant exhibit a two-state unfolding transition at mildly acidic conditions (pH = 5–7), with a decrease in molar ellipticity at 220 nm indicating a loss of α-helical content at acidic pH. The UV spectra for the rHb1 WT and H73L mutant show the presence of the Soret band [8] absorbance maxima at 410 and 395 nm, respectively, regardless of the solution pH. That is, changes in the solution pH do not affect the position of the Soret band maxima indicating that the environment of the heme prosthetic group is not significantly altered despite the decrease in α-helical content in the WT and H73L mutant upon acidification. The rHb1 WT protein showed Q-bands at 537 and 573 nm indicating the protein to be hexacoordinate, while the H73L mutant is pentacoordinate and exhibits a single Q-band at 500 nm due to the inability of leucine to form a coordination bond with the heme iron. Moreover, changes in the absorption band at 280 nm as a function of solution pH are observed for the rHb1 H73L mutant while no changes are observed for the WT. This result suggests that as the pH decreases, one or more tryptophan residues (Trp25, Trp138, and Trp146 located at N- and C-terminal α-helices A and H, see Fig. S1) are exposed to the bulk solvent and thus the N- and C-terminal α-helices in the rHb1 H73L mutant are destabilized during acid unfolding, in good agreement with the increase of the apo form as the pH decreases observed in the nESI-TIMS-TOF MS analysis (Fig. 1).

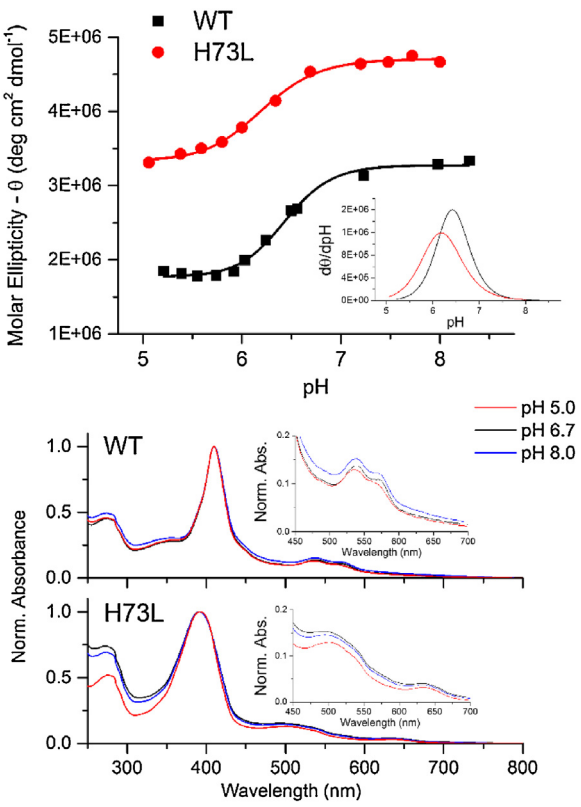

Fig. 2. (Top) Molar ellipticity at 220 nm determined by circular dichroism as a function of the pH for rHb1 WT (black) and H73L (red) in 10 mM ammonium acetate buffer. Inset: The first derivative indicates similar unfolding transition with the pH for rHb1 WT (black) and H73L (red). (Bottom) UV spectra of protein samples at pH 5.0 (red), 6.7 (black), and 8.0 (blue) and. Absorbance values are normalized to the Soret band intensity. (For interpretation of the references to colour in this figure legend, the reader is referred to the web version of this article.)

Multiple mobility bands were observed per charge state for the rHb1 WT and H73L mutant (Figs. 3 and 4, respectively). The high resolution of the TIMS analyzer permitted the separation of a large number of kinetic intermediates and a potential contribution of higher order oligomers was ruled out using a dilution series comparison (see Fig. S2). As a general trend, a kinetic intermediate can be observed over a range of charge states and an unfolding transition between kinetic intermediates is typically associated with an increase in the charge state and the Ω values. Comparison of the mobility profiles for rHb1 WT and H73L mutant showed a similar trend in the kinetic intermediate distribution (Fig. S3); however, closer inspection shows the largest difference in the presence of low charge states and smaller Ω mobility bands as a function of the solution pH. We interpret this result to be due to the higher stability of the rHb1 WT, which retains a greater degree of native structure at mildly acidic conditions compared to the H73L mutant. Representa-

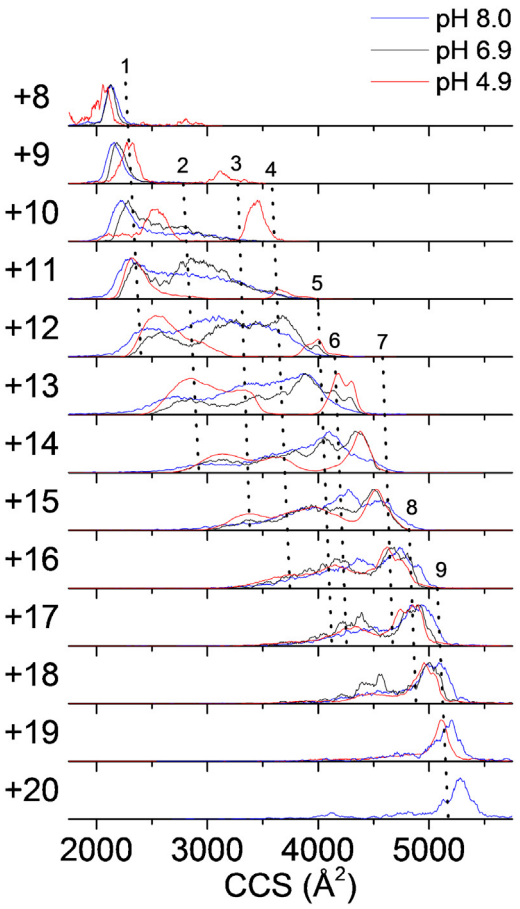

Fig. 3. Typical mobility profiles for rHb1 WT using nESI-TIMS-TOF MS as a function of the starting solution pH 8.0 (blue), 6.9 (black), and pH 4.9 (red). Numbered, dotted black lines correspond to the CCS values of the unfolding representative rHb1 candidate structures contained in Fig. 5. Data were acquired at a scan rate ($S_r = \Delta V_{ramp}/t_{ramp}$) of $S_r = 2.8$ V/ms. (For interpretation of the references to colour in this figure legend, the reader is referred to the web version of this article.)

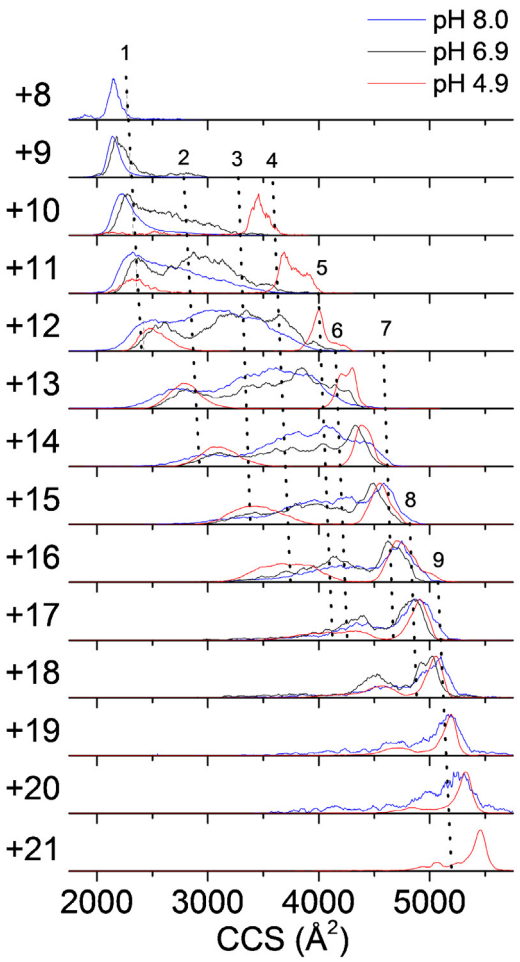

Fig. 4. Typical mobility profiles for rHb1 H73L using nESI-TIMS-TOF MS as a function of the starting solution pH 8.0 (blue), 6.9 (black), and pH 4.9 (red). Numbered, dotted black lines correspond to the CCS values of the unfolding representative rHb1 candidate structures contained in Fig. 5. Data were acquired at a scan rate ($S_r = \Delta V_{ramp}/t_{ramp}$) of $S_r = 2.8$ V/ms. (For interpretation of the references to colour in this figure legend, the reader is referred to the web version of this article.)

tive candidate structures of the main Ω transitions were proposed based on our spectroscopic data and typical globin unfolding pathways and their Ω are provided as a function of the charge state (Fig. 5 and Table S2). Closer inspection of Figs. 3 and 4 shows that a good agreement is observed between the proposed representative structure and the Ω unfolding transitions. For example, the similarity between the theoretical Ω determined for the representative candidate structure of the native state (#1) and the lower Ω mobility bands (~2100 Å^2) observed at low charge states (+8–+10) suggests that these bands correspond to conformational states very close to the native form that retain the 3-over-3 α-helical globin fold structure and are therefore most relevant to the biological activity of the proteins in their native state. The width of these individual mobility bands is indicative of structural heterogeneity originating in the solution phase and is similar to that observed previously for myoglobin [28]. Under these experimental conditions, a typical resolving power of 150–250 is expected for a single conformer. Major differences in the Ω of the native rHb1 WT and H73L mutant are not observed, which suggest that their tridimensional structures are very similar probably due to the small contribution of the heme cavity to the overall tridimensional structure.

Closer inspection of the lower charge states (+8–+10) for rHb1 WT and H73L showed a small dependence on the starting solution pH (Fig. 3 and 4). The changes (<6%) in Ω for the native-like rHb1 may be associated with the protonation of basic residues (e.g., distal His73, His117, and His152, pK_a of 6.6 ± 1.0 [45]) at more acidic pH which slightly alters the native-like conformation and the environment of the heme prosthetic group. This observation agrees with computational results which showed changes in the protein structure due to protonation of the aforementioned His residues [8] and supports the idea that pH plays a role in the activity of the protein *in vivo*. Comparison of the rHb1 WT and H73L mobility profiles of the holo- and apo- form showed that only the initial unfolding pathways involves the heme cavity (Fig. S4 and S5), with and without a heme loss, followed by unfolding pathways not necessarily involving the environment of the heme prosthetic group.

A potential unfolding pathway is proposed using candidate structures characteristic of the Ω ensemble and the UV and CD analysis (see Fig. 5). Under this approximation, initial unfolding involves distancing of the A- and H-helices at the N- and C-terminal (structures #2 and # 3), followed by distancing of the B-helix (structure # 4). The resulting loops are then further remodeled to reflect the impact of Coulombic repulsion between unfolded regions of the protein at higher charge states (structure #5 and #6). Accessing theoretical Ω values higher than ~4200 Å^2 requires dissociation of the distal histidine and α-helices which form the core of the protein near the heme group (structure # 7) followed by further unfolding of secondary structural elements and remodeling of the polypeptide chain to represent Coulombic repulsion (structures #8 and #9). RMSD values from sequential representative transition

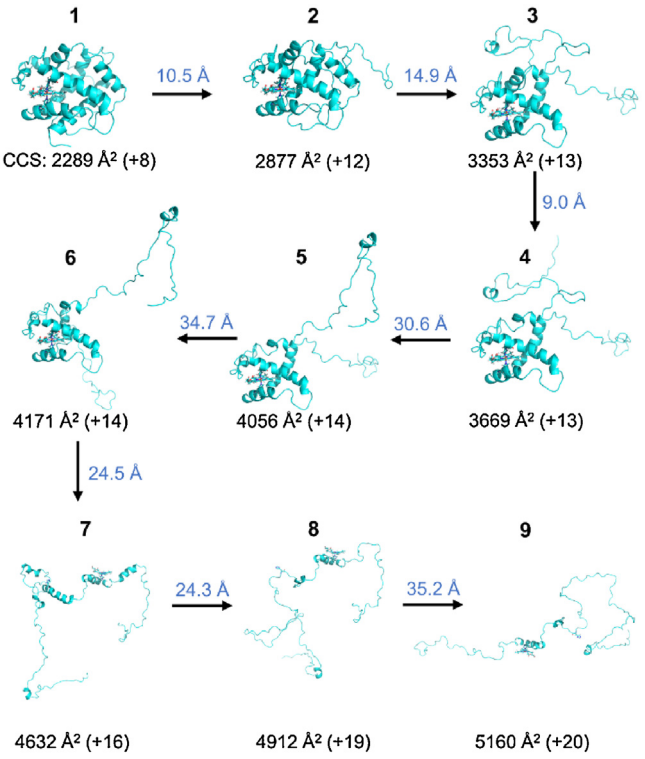

Fig. 5. Representative rHb1 structures of the main unfolding transitions obtained using molecular dynamics and their changes (RMSD) with respect to the previous candidate structure. Theoretical CCS values are shown for the most abundant charge states observed experimentally.

structures are indicative of the denaturation and distancing of the helices from the environment of the heme prosthetic group, particularly upon unfolding of the G-helix and dissociation of the core EF-helical region. The largest Ω mobility bands we observe likely correspond to the fully unfolded random coil forms of rHb1 WT and H73L; candidate structures retaining native secondary and tertiary structural elements are unable to access Ω values greater than ~5000 Å^2. It must be stressed that these candidate structures are not provided as unique assignments of particular mobility bands, but as an attempt to describe one of the potential pathways, guided by the Ω ensemble, spectroscopic data and previously-determined unfolding pathways for heme proteins. The vast structural heterogeneity and flexibility involved during the unfolding – as evidenced by the broad mobility bands of rHb1 WT and H73L mutant – makes the candidate definitive assignment of all kinetic intermediates challenging.

4. Conclusion

The high resolving power of the TIMS analyzer combined with molecular dynamics simulation permitted, for the first time, the study of the kinetic intermediates of rHb1 as a function of the solution pH. The nESI-TIMS-MS analysis of rHb1 WT and H73L as a function of the starting solvent conditions (pH = 4.9–8.0) showed a wide charge state distribution (i.e., +8–+21 charge states) and a wide Ω range (2000–5500 Å^2). Experimental results showed that mildly acidic conditions can disrupt the intramolecular interactions that stabilized the native state and that the hexacoordinate rHb1 WT has higher stability against unfolding in comparison to the H73L mutant and horse myoglobin. Inspection of the molar ellipticity (θ) and its first derivative (dθ/dpH) showed that rHb1 WT and H73L mutant exhibit a two-state unfolding transition at mildly acidic conditions (pH = 5–7), with a decrease in molar ellipticity at 220 nm indicating a loss of α-helical content. The nESI-TIMS-TOF MS experiments enabled us to establish a general trend where the trapped intermediates increase in Ω as a function of the charge state and that the solution "native" states are retained in the gas-phase. Based on the UV, CD and mobility profiles, representative candidate structures were proposed for the nine transitions observed in the mobility profiles. The described pathway suggests that rHb1 unfolding involves an initial distancing of the A, B, and H helices, while the core of the protein structure containing the heme cavity and heme group remains mostly intact, followed by the distancing of the E, F, and G helices and subsequent loss of the α-helical structure leading to a final random coil conformation.

Declaration of competing interest

The authors declare no competing interests.

Acknowledgements

This work was supported by a National Science Foundation Division of Chemistry, under CAREER award CHE-1654274, with co-funding from the Division of Molecular and Cellular Biosciences to F.F.-L. The authors would also like to acknowledge the helpful discussions and technical support from Dr. Mark E. Ridgeway and Dr. Melvin A. Park from Bruker Daltonics Inc. during the development and installation of the custom-built TIMS-TOF MS instrument.

Appendix A. Supplementary data

Supplementary data associated with this article can be found, in the online version, at https://doi.org/10.1016/j.ijms.2018.03.008.

References

[1] R. Arredondo-Peter, M.S. Hargrove, G. Sarath, J.F. Moran, J. Lohrman, J.S. Olson, R.V. Klucas, Rice hemoglobins. Gene cloning, analysis, and O2-binding kinetics of a recombinant protein synthesized in Escherichia coli, Plant Physiol. 115 (1997) 1259–1266.
[2] M.S. Hargrove, E.A. Brucker, B. Stec, G. Sarath, R. Arredondo-Peter, R.V. Klucas, J.S. Olson, G.N. Phillips, Crystal structure of a nonsymbiotic plant hemoglobin, Structure 8 (2000) 1005–1014.
[3] J.B. Wittenberg, F.J. Bergersen, C.A. Appleby, G.L. Turner, Facilitated oxygen diffusion: the role of leghemoglobin in nitrogen fixation by bacteroids isolated from soybean root nodules, J. Biol. Chem. 249 (1974) 4057–4066.
[4] B.J. Smagghe, J.T. Trent III, M.S. Hargrove, NO dioxygenase activity in hemoglobins is ubiquitous in vitro, but limited by reduction in vivo, PLoS One 3 (2008) e2039.
[5] M.A. Gilles-Gonzalez, G. Gonzalez, M.F. Perutz, L. Kiger, M.C. Marden, C. Poyart, Heme-based sensors, exemplified by the kinase FixL, are a new class of heme protein with distinctive ligand binding and autoxidation, Biochemistry 33 (1994) 8067–8073.
[6] E.J.H. Ross, L. Shearman, M. Mathiesen, Y.J. Zhou, R. Arredondo-Peter, G. Sarath, R.V. Klucas, Nonsymbiotic hemoglobins in rice are synthesized during germination and in differentiating cell types, Protoplasma 218 (2001) 125–133.
[7] V. Lira-Ruan, G. Sarath, R.V. Klucas, R. Arredondo-Peter, Synthesis of hemoglobins in rice (Oryza sativa var. Jackson) plants growing in normal and stress conditions, Plant Sci. 161 (2001) 279–287.
[8] D. Butcher, S. Bernad, V. Derrien, P. Sebban, J. Miksovska, Role of ionic strength and pH in modulating thermodynamic profiles associated with CO escape from rice nonsymbiotic hemoglobin 1, J. Phys. Chem. B 121 (2017) 351–364.
[9] H.H. Felle, pH: signal and messenger in plant cells, Plant Biol. 3 (2001) 577–591.
[10] F. Fernandez-Lima, D.A. Kaplan, J. Suetering, M.A. Park, Gas-phase separation using a trapped ion mobility spectrometer, Int. J. Ion Mobility Spectrom. 14 (2011) 93–98.
[11] F.A. Fernandez-Lima, D.A. Kaplan, M.A. Park, Note Integration of trapped ion mobility spectrometry with mass spectrometry, Rev. Sci. Instrum. 82 (2011) 126106.
[12] A. Castellanos, P. Benigni, D.R. Hernandez, J.D. DeBord, M.E. Ridgeway, M.A. Park, F. Fernandez-Lima, Fast screening of polycyclic aromatic hydrocarbons using trapped ion mobility spectrometry – mass spectrometry, Anal. Methods 6 (2014) 9328–9332.
[13] J.C. Molano-Arevalo, D.R. Hernandez, W.G. Gonzalez, J. Miksovska, M.E. Ridgeway, M.A. Park, F. Fernandez-Lima, Flavin adenine dinucleotide

structural motifs: from solution to gas phase, Anal. Chem. 86 (2014) 10223–10230.
[14] E.R. Schenk, V. Mendez, J.T. Landrum, M.E. Ridgeway, M.A. Park, F. Fernandez-Lima, Direct observation of differences of carotenoid polyene chain cis/trans isomers resulting from structural topology, Anal. Chem. 86 (2014) 2019–2024.
[15] E.R. Schenk, M.E. Ridgeway, M.A. Park, F. Leng, F. Fernandez-Lima, Isomerization kinetics of AT hook decapeptide solution structures, Anal. Chem. 86 (2014) 1210–1214.
[16] P. Benigni, C.J. Thompson, M.E. Ridgeway, M.A. Park, F. Fernandez-Lima, Targeted high-resolution ion mobility separation coupled to ultrahigh-Resolution mass spectrometry of endocrine disruptors in complex mixtures, Anal. Chem. 87 (2015) 4321–4325.
[17] A. McKenzie-Coe, J.D. DeBord, M. Ridgeway, M. Park, G. Eiceman, F. Fernandez-Lima, Lifetimes and stabilities of familiar explosive molecular adduct complexes during ion mobility measurements, Analyst 140 (2015) 5692–5699.
[18] K.J. Adams, D. Montero, D. Aga, F. Fernandez-Lima, Isomer separation of polybrominated diphenyl ether metabolites using nanoESI-TIMS-MS, Int. J. Ion Mobility Spectrom. 19 (2016) 69–76.
[19] P. Benigni, R. Marin, J.C. Molano-Arevalo, A. Garabedian, J.J. Wolff, M.E. Ridgeway, M.A. Park, F. Fernandez-Lima, Towards the analysis of high molecular weight proteins and protein complexes using TIMS-MS, Int. J. Ion Mobility Spectrom. 19 (2016) 95–104.
[20] Y. Pu, M.E. Ridgeway, R.S. Glaskin, M.A. Park, C.E. Costello, C. Lin, Separation and identification of isomeric glycans by selected accumulation-trapped ion mobility spectrometry-electron activated dissociation tandem mass spectrometry, Anal. Chem. 88 (2016) 3440–3443.
[21] J.A. Silveira, W. Danielson, M.E. Ridgeway, M.A. Park, Altering the mobility-time continuum: nonlinear scan functions for targeted high resolution trapped ion mobility-mass spectrometry, Int. J. Ion Mobility Spectrom. 19 (2016) 87–94.
[22] J.A. Silveira, M.E. Ridgeway, F.H. Laukien, M. Mann, M.A. Park, Parallel accumulation for 100% duty cycle trapped ion mobility-mass spectrometry, Int. J. Mass spectrom. 413 (2017) 168–175.
[23] P. Benigni, F. Fernandez-Lima, Oversampling selective accumulation trapped ion mobility spectrometry coupled to FT-ICR MS: fundamentals and applications, Anal. Chem. 88 (2016) 7404–7412.
[24] P. Benigni, K. Sandoval, C.J. Thompson, M.E. Ridgeway, M.A. Park, P. Gardinali, F. Fernandez-Lima, Analysis of photoirradiated water accommodated fractions of crude oils using tandem TIMS and FT-ICR MS, Environ. Sci. Technol. 51 (2017) 5978–5988.
[25] A. Garabedian, D. Butcher, J.L. Lippens, J. Miksovska, P. Chapagain, D. Fabris, M.E. Ridgeway, M.A. Park, F. Fernandez-Lima, Structures of the kinetically trapped i-motif DNA intermediates, Phys. Chem. Chem. Phys. 18 (2016) 26691–26702.
[26] M.E. Ridgeway, J.A. Silveira, J.E. Meier, M.A. Park, Microheterogeneity within conformational states of ubiquitin revealed by high resolution trapped ion mobility spectrometry, Analyst 140 (2015) 6964–6972.
[27] F.C. Liu, S.R. Kirk, C. Bleiholder, On the structural denaturation of biological analytes in trapped ion mobility spectrometry – mass spectrometry, Analyst 141 (2016) 3722–3730.
[28] E.R. Schenk, R. Almeida, J. Miksovska, M.E. Ridgeway, M.A. Park, F. Fernandez-Lima, Kinetic intermediates of holo- and apo-myoglobin studied using HDX-TIMS-MS and molecular dynamics simulations, J. Am. Soc. Mass Spectrom. 26 (2015) 555–563.
[29] J.C. Molano-Arevalo, K. Jeanne Dit Fouque, K. Pham, J. Miksovska, M.E. Ridgeway, M.A. Park, F. Fernandez-Lima, Characterization of intramolecular interactions of cytochrome c using hydrogen–deuterium exchange-trapped ion mobility spectrometry–mass spectrometry and molecular dynamics, Anal. Chem. 89 (2017) 8757–8765.
[30] F. Fernandez-Lima, Trapped Ion Mobility Spectrometry: past, present and future trends, Int. J. Ion Mobility Spectrom. 19 (2016) 65–67.
[31] D.R. Hernandez, J.D. DeBord, M.E. Ridgeway, D.A. Kaplan, M.A. Park, F. Fernandez-Lima, Ion dynamics in a trapped ion mobility spectrometer, Analyst 139 (2014) 1913–1921.
[32] E.W. McDaniel, E.A. Mason, Mobility and Diffusion of Ions in Gases, John Wiley and Sons, Inc., New York New York, 1973.
[33] W.D. Cornell, P. Cieplak, C.I. Bayly, I.R. Gould, K.M. Merz, D.M. Ferguson, D.C. Spellmeyer, T. Fox, J.W. Caldwell, P.A. Kollman, A second generation force field for the simulation of proteins, nucleic acids, and organic molecules, J. Am. Chem. Soc. 117 (1995) 5179–5197.
[34] E.R. Schenk, F. Nau, F. Fernandez-Lima, Theoretical predictor for candidate structure assignment from IMS data of biomolecule-related conformational space, Int. J. Ion Mobility Spectrom. 18 (2015) 23–29.
[35] F.A. Fernandez-Lima, H. Wei, Y.Q. Gao, D.H. Russell, On the structure elucidation using ion mobility spectrometry and molecular dynamics, J. Phys. Chem. A 113 (2009) 8221–8234.
[36] S.A. Ewing, M.T. Donor, J.W. Wilson, J.S. Prell, Collidoscope: an improved tool for computing collisional cross-Sections with the trajectory method, J. Am. Soc. Mass Spectrom. 28 (2017) 587–596.
[37] S. Vahidi, B.B. Stocks, L. Konermann, Partially disordered proteins studied by ion mobility-mass spectrometry: implications for the preservation of solution phase structure in the gas phase, Anal. Chem. 85 (2013) 10471–10478.
[38] K.B. Shelimov, M.F. Jarrold, Conformations, unfolding, and refolding of apomyoglobin in vacuum: an activation barrier for gas-phase protein folding, J. Am. Chem. Soc. 119 (1997) 2987–2994.
[39] S.J. Valentine, D.E. Clemmer, H.D. Temperature-dependent, Temperature-dependent H/D exchange of compact and elongated cytochrome c ions in the gas phase, J. Am. Soc. Mass Spectrom. 13 (2002) 506–517.
[40] S.J. Allen, R.M. Eaton, M.F. Bush, Structural dynamics of native-Like ions in the gas phase: results from tandem ion mobility of cytochrome c, Anal. Chem. 89 (2017) 7527–7534.
[41] K.J. Laszlo, J.H. Buckner, E.B. Munger, M.F. Bush, Native-like and denatured cytochrome c ions yield cation-to-anion proton transfer reaction products with similar collision cross-sections, J. Am. Soc. Mass Spectrom. 28 (2017) 1382–1391.
[42] F. Fernandez-Lima, R.C. Blase, D.H. Russell, A study of ion-neutral collision cross section values for low charge states of peptides, proteins, and peptide/protein complexes, Int. J. Mass Spectrom. 298 (2011) 111–118.
[43] I.A. Kaltashov, C.E. Bobst, R.R. Abzalimov, G. Wang, B. Baykal, S. Wang, Advances and challenges in analytical characterization of biotechnology products: mass spectrometry-based approaches to study properties and behavior of protein therapeutics, Biotechnol. Adv. 30 (2012) 210–222.
[44] L. Konermann, Addressing a common misconception: ammonium acetate as neutral pH buffer for native electrospray mass spectrometry, J. Am. Soc. Mass Spectrom. 28 (2017) 1827–1835.
[45] G.R. Grimsley, J.M. Scholtz, C.N. Pace, A summary of the measured pK values of the ionizable groups in folded proteins, Protein Sc.: Publ. Protein Soc. 18 (2009) 247–251.